Dalton Transactions

PAPER

View Article Online
View Journal | View Issue

Cite this: *Dalton Trans.*, 2016, **45**, 5262

$BaAl_4$ derivative phases in the sections {La,Ce}-Ni_2Si_2–{La,Ce}Zn_2Si_2: phase relations, crystal structures and physical properties†‡

Fainan Failamani,[a] Zahida Malik,§[a] Leonid Salamakha,[b] Friedrich Kneidinger,[b] Andriy Grytsiv,[a,c] Herwig Michor,[b] Ernst Bauer,[b,c] Gerald Giester[d] and Peter Rogl*[a,c]

Received 1st December 2015,
Accepted 6th February 2016

DOI: 10.1039/c5dt04705f

www.rsc.org/dalton

Phase relations and crystal structures have been evaluated within the sections $LaNi_2Si_2$–$LaZn_2Si_2$ and $CeNi_2Si_2$–$CeZn_2Si_2$ at 800 °C using electron microprobe analysis and X-ray powder and single crystal structure analyses. Although the systems La–Zn–Si and Ce–Zn–Si at 800 °C do not reveal compounds such as "$LaZn_2Si_2$" or "$CeZn_2Si_2$", solid solutions {La,Ce}$(Ni_{1-x}Zn_x)_2Si_2$ exist with the Ni/Zn substitution starting from {La,Ce}Ni_2Si_2 ($ThCr_2Si_2$-type; *I*4/*mmm*) up to x = 0.18 for $Ce(Ni_{1-x}Zn_x)_2Si_2$ and x = 0.125 for $La(Ni_{1-x}Zn_x)_2Si_2$. For higher Zn-contents $0.25 \le x \le 0.55$ the solutions adopt the $CaBe_2Ge_2$-type (*P*4/*nmm*). The investigations are backed by single crystal X-ray diffraction data for $Ce(Ni_{0.61}Zn_{0.39})_2Si_2$ (*P*4/*nmm*; a = 0.41022(1) nm, c = 0.98146(4) nm; R_F = 0.012) and by Rietveld refinement for $La(Ni_{0.56}Zn_{0.44})_2Si_2$ (*P*4/*nmm*; a = 0.41680(6) nm, c = 0.99364(4) nm; R_F = 0.043). Interestingly, the Ce–Zn–Si system contains a ternary phase $CeZn_2(Si_{1-x}Zn_x)_2$ of the $ThCr_2Si_2$ structure type ($0.25 \le x \le 0.30$ at 600 °C), which forms peritectically at T = 695 °C but does not include the composition "$CeZn_2Si_2$". The primitive high temperature tetragonal phase with the $CaBe_2Ge_2$-type has also been observed for the first time in the Ce–Ni–Si system at $CeNi_{2+x}Si_{2-x}$, x = 0.33 (single crystal data, *P*4/*nmm*; a = 0.40150(2) nm, c = 0.95210(2) nm; R_F = 0.0163). Physical properties (from 400 mK to 300 K) including specific heat, electrical resistivity and magnetic susceptibility have been elucidated for $Ce(Ni_{0.61}Zn_{0.39})_2Si_2$ and $La(Ni_{0.56}Zn_{0.44})_2Si_2$. $Ce(Ni_{0.61}Zn_{0.39})_2Si_2$ exhibits a Kondo-type ground state. Low temperature specific heat data of $La(Ni_{0.56}Zn_{0.44})_2Si_2$ suggest a spin fluctuation scenario with an enhanced value of the Sommerfeld constant.

1. Introduction

Since its discovery in 1935 by Andress and Alberti,[1] the $BaAl_4$ structure type and its derivatives have been found in more than 200 intermetallic compounds, particularly the three tetragonal ternary variants: the $ThCr_2Si_2$-type by Ban and Sikirica[2] (or $CeAl_2Ga_2$-type discovered independently by Zarechnyuk *et al.*[3] in the same year), $CaBe_2Ge_2$ by Eisenmann *et al.*[4] and the non-centrosymmetric variant $BaNiSn_3$ by Dörrscheidt and Schäfer.[5] The $BaAl_4$ structure type furthermore is one of the building blocks of various structure types, such as $U_3Ni_4Si_4$, $CeNiSi_2$ (in combination with AlB_2-type slabs) and many others.[6]

Although phase equilibria in the Ce–Ni–Si system were investigated in the 70s by Bodak *et al.*[7,8] more ternary phases were discovered afterwards: $Ce_2Ni_3Si_5$ ($U_2Co_3Si_5$-type, orthorhombic superstructure variant of $BaAl_4$),[9] $Ce_{14}Ni_6Si_{11}$,[10] Ce_3NiSi_3,[11] *etc*. Being the last member of the first row of transition metals, Zn containing ternary rare earth silicon systems had been one of the least investigated types of systems. Only some reports on the formation of ternary compounds could be found in the literature.[12] Recently our report[13] on the Ce–Zn–Si system at 800 °C revealed the formation of several ternary phases. Surprisingly neither $BaAl_4$ nor its derivative structure could be found in the system at 800 °C, instead a far off-stoichiometric $ThCr_2Si_2$-type $CeZn_{2+x}Si_{2-x}$ ($x \sim 0.5$, labelled as τ_6) was found to be stable at temperatures below 695 ± 5 °C.[14]

Compounds crystallizing in the $BaAl_4$ type or its derivatives are often associated with various exotic superconducting

[a]*Institute of Materials Chemistry and Research, University of Vienna, Währingerstraße 42, A-1090 Vienna, Austria. E-mail: fai.failamani@gmail.com, zahida.malik@sns.nust.edu.pk, andriy.grytsiv@univie.ac.at, peter.franz.rogl@univie.ac.at; Fax: +43 142779524; Tel: +43 1427752456*
[b]*Institute of Solid State Physics, TU Wien, Wiedner Hauptstraße 8–10, A-1040 Vienna, Austria. E-mail: salamakhaleonid@rambler.ru, kneidinger@ifp.tuwien.ac.at, michor@ifp.tuwien.ac.at, bauer@ifp.tuwien.ac.at; Fax: +43 15880113199; Tel: +43 15880113160*
[c]*Christian Doppler Laboratory for Thermoelectricity, Vienna, Austria*
[d]*Institute of Mineralogy and Crystallography, University of Vienna, Althanstraße 14, A-1090 Vienna, Austria. E-mail: gerald.giester@univie.ac.at; Fax: +43 14277853235; Tel: +43 1427753235*

† Dedicated to Prof. Dr Wolfgang Jeitschko on the occasion of his 80th birthday.

‡ Electronic supplementary information (ESI) available. See DOI: 10.1039/c5dt04705f

§ Present address: Department of Chemistry, SNS, NUST, H-12, Islamabad, Pakistan.

phenomena, starting with the discovery of heavy fermion superconductivity in $CeCu_2Si_2$ by Steglich *et al.* in 1979,[15] which breaks the previous belief of non-coexistence between magnetism and superconductivity. Spin density wave transition was found in $BaFe_2As_2$,[16] followed by the discovery of superconductivity in K-doped[17] and Co-doped $BaFe_2As_2$.[18] More recently, BCS-like superconductivity was found in non-centrosymmetric $BaPtSi_3$ ($BaNiSn_3$-type)[19] and isotypes.[20]

In cerium and actinoid compounds the hybridization of the Ce-f electrons with the conduction band gives rise to various kinds of interesting physical phenomena. Systematic studies of the transport, magnetic and calorimetric properties and Ce L_{III} X-ray absorption spectra and XPS measurements characterized $CeNi_2Si_2$ as an intermediate valence (valence fluctuation) system with a characteristic Kondo-lattice temperature $T^* \sim 600$ K.[21–26] The positive Seebeck coefficient, decreasing with the Si content in $CeNi_{2-x}Si_{2+x}$ was taken as a decrease of the electronic DOS particularly of the Ni-3d-states at the Fermi level concomitant with a narrowing of the Ce-4f level and a decreasing Ce-valence.[27] The replacement of Ni by Pd, Cu, Au drives the Ce from an intermediate valence (IV) to a non-IV ground state.[21–27] Probably because of the non-existence of compounds "$LaZn_2Si_2$" and "$CeZn_2Si_2$", the corresponding isopleths {La,Ce}Ni_2Si_2–{La,Ce}Zn_2Si_2 have not attracted interest.

Therefore the present work intends to provide detailed information on the phase equilibria, crystal structures and physical properties of the novel $BaAl_4$-derivative phases in the systems {La,Ce}–Ni–Si as well as in the isopleths {La,Ce}Ni_2Si_2–{La,Ce}Zn_2Si_2.

2. Experimental

Samples were prepared from cerium ingots (Alfa Aesar, purity >99.9 mass%), lanthanum ingots (Auer Remy, 99.9 mass%), zinc granules (Alfa Aesar, >99.9 mass%), Ni foil (Alfa Aesar, >99.8 mass%) and silicon pieces (Alfa Aesar, 6N). Zinc drops were purified in an evacuated quartz tube by heating them at ~750 °C, below the boiling point of Zn (907 °C). Cerium and lanthanum ingots were mechanically surface cleaned before use.

Polycrystalline bulk samples for the analysis of the quaternary isopleths {La,Ce}$(Ni_{1-x}Zn_x)_2Si_2$ and for physical property studies were prepared from intimate blends of powders of arc melted master alloys {La,Ce}$Ni_{2-x}Si_2$ (various x; powdered under cyclohexane) and fine Zn-filings in appropriate compositional ratios. These blends were cold compacted in a steel die without lubricants, vacuum-sealed in quartz tubes, heated from 420 °C to 800 °C at the rate of 1 °C min^{-1} and then annealed at this temperature for 7 days. After water quenching the samples were re-powderized (under cyclohexane) in order to ensure homogeneity. The samples were loaded into 10 mm diameter graphite dies for hot pressing under Ar in a uniaxial hot press system (HP W 200/250-2200-200-KS) at 800 °C for 1 hour employing a pressure of 56 MPa. Densities of the samples have been calculated from their dimensions and masses after removing a 0.5 mm thick surface layer (grinding with SiC paper).

X-ray powder diffraction data were collected from each alloy employing a Guinier–Huber image plate system with monochromatic $CuK_{\alpha 1}$ radiation ($8° < 2\theta < 100°$). Precise lattice parameters were calculated by least squares fits to the indexed 2θ values calibrated with Ge as the internal standard (a_{Ge} = 0.565791 nm). Quantitative Rietveld refinements of the X-ray powder diffraction data were performed with the FULLPROF program.[28]

Single crystals from the systems {La,Ce}–Ni–Si were picked from crushed reguli. Quaternary single crystals were grown from Zn flux starting from a cold compacted pellet ($Ce_2Ni_4Si_8$ + Zn-filings = $Ce_2Ni_4Si_8Zn_{86}$ (in at.%)), which was heated to 900 °C at the rate of 1 °C min^{-1} and then cooled to 800 °C at the same rate. After annealing for 4 days at this temperature the sample was subsequently quenched in water and then boiled with 15% aqueous solution of HCl in a water bath in order to dissolve the extra Zn. Crystals were carefully washed with distilled water and dried.

Inspections on an AXS-GADDS texture goniometer assured the high crystal quality, unit cell dimensions and Laue symmetry of the specimens prior to the X-ray intensity data collections on a four-circle Nonius Kappa diffractometer equipped with a CCD area detector employing graphite monochromated MoKα radiation (λ = 0.071069 nm). Orientation matrices and unit cell parameters were derived using the program DENZO.[29] Besides the general treatment of absorption effects using the multi-scan technique (redundancy of integrated reflections >8) no additional absorption corrections were performed because of the rather regular crystal shapes and small dimensions of the investigated specimens. The structures were solved by direct methods and were refined with the SHELXL-97 program[30] within the Windows version WinGX.[31]

After the reaction during annealing the samples had almost a powder-like consistency, too soft to be polished by standard procedures. This problem was overcome by casting the sample powder along with conducting glue into a cylindrical mould of ~5 mm diameter. After hardening several of the powder cylinders were hot compacted in conductive resin and were ground and polished under glycerine instead of water in order to avoid oxidation of the samples. Microstructures and compositions were examined by light optical microscopy (LOM) and scanning electron microscopy (SEM) *via* Electron Probe Micro-Analyses (EPMA) on a Zeiss Supra 55 VP equipped with an EDX system operated at 20 kV.

Physical property measurements (magnetic susceptibility, electrical resistivity, and specific heat) were performed on the hot pressed samples with methods described in our previous publications, *e.g.* ref. 32.

3. Results and discussion

3.1. The $BaAl_4$-type derivative phases in the systems La–Ni–Si and Ce–Ni–Si

The system Ce–Ni–Si relevant to this work was investigated by Bodak and coworkers.[7,8] The isothermal section of La–Ni–Si at 400 °C was established much later by Zhou *et al.*[33] Both

systems contain a compound $\{La,Ce\}Ni_2Si_2$ which was reported to crystallize in the $ThCr_2Si_2$ type[34] with a practically negligible homogeneity range. A thorough check on these findings prompted us to prepare samples with the nominal composition $\{La,Ce\}_{20}Ni_{40}Si_{40}$ (in at.%). As-cast alloys as well as samples annealed at 800 °C for 4 days revealed nearly a single phase condition with the $ThCr_2Si_2$ type, thus suggesting a congruent or a degenerate peritectic formation of these phases, and furthermore confirmed the crystal structure data from Bodak *et al.*[34] Levin *et al.*[27] studied the homogeneity range of $CeNi_2Si_2$ ($ThCr_2Si_2$-type) at a relatively low temperature of 727 °C and discovered a rather large homogeneity range of 8 at.% ranging from 36 to 44 at.% Si. Our reinvestigation (EPMA) of the phase relations around $CeNi_2Si_2$ at 800 °C reveals a smaller homogeneity range for the $ThCr_2Si_2$ type of ~4 at.% from 38.3 to 42.3 at.% Si. Our lattice parameters (see Fig. 1), however, agree well with the result of Levin *et al.*[27] In general the Ni/Si substitution does not affect the *a*-axis much, however one can see that the *c*-axis decreases almost linearly with increasing Ni content. In an attempt to investigate the crystal structure of $CeNi_4Si$[35] we discovered a Ni-rich phase $CeNi_{2+x}Si_{2-x}$ ($x \sim 0.3$). EPM analysis of an as-cast alloy with a slightly higher Ni-content ($Ce_{20}Ni_{43}Si_{37}$) showed primary crystallization of $Ce_{20}Ni_{41}Si_{39}$ followed by a peritectic-like formation of a thin layer of $Ce_{20}Ni_{46}Si_{34}$ (see Fig. 2). The remaining liquid crystallized as $CeNi_4Si$ and a novel phase

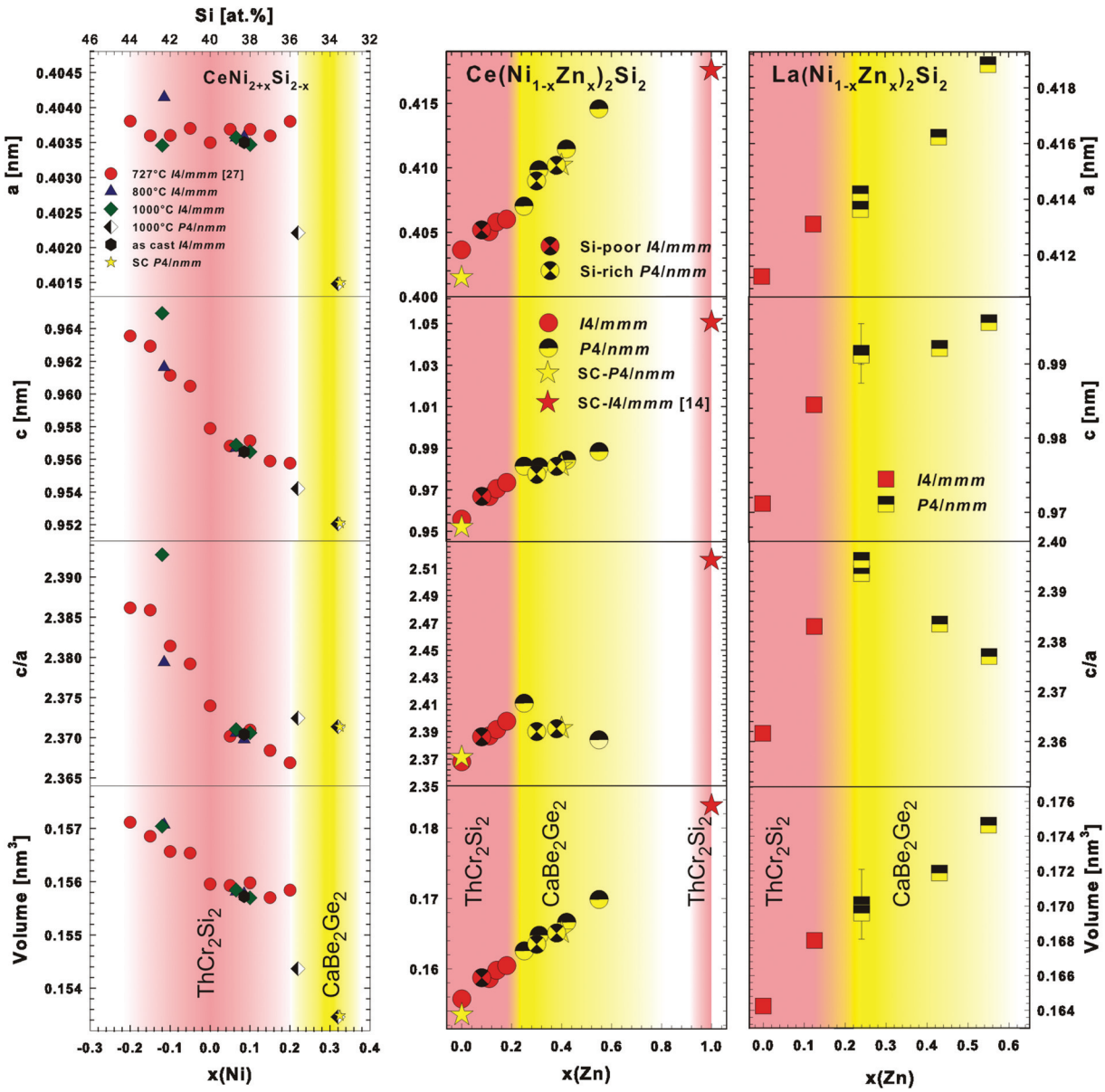

Fig. 1 Left column: compositional dependence of lattice parameters of $CeNi_{2+x}Si_{2-x}$. Right two columns: unit cell parameters *vs.* Zn-content in the $BaAl_4$-type phases $\{La,Ce\}[Ni_{1-x}Zn_x]_2Si_2$ (annealed at 800 °C) revealing a transition from the body centred to primitive symmetry as a consequence of Ni/Zn substitution (compositions from EPMA).

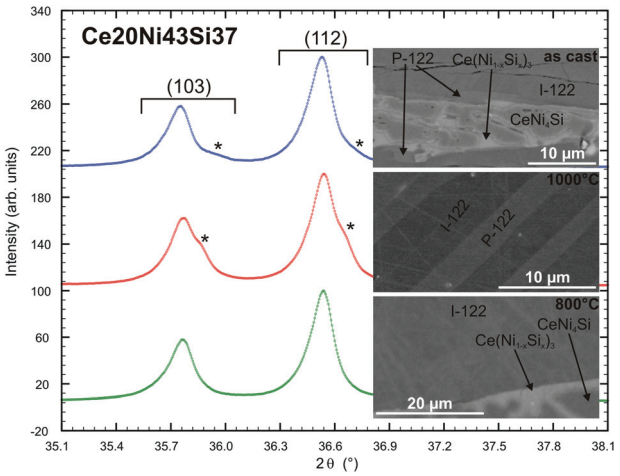

Fig. 2 The strongest $BaAl_4$-type reflections and the micrograph of the $Ce_{20}Ni_{43}Si_{37}$ alloy in as-cast conditions, annealed at 1000 °C and at 800 °C. The asterisks represent the $CaBe_2Ge_2$-type reflections (see section 3.1.1 for detailed explanation).

$Ce(Ni_{1-x}Si_x)_3$. Besides the main reflections arising from the $ThCr_2Si_2$-type ($Ce_{20}Ni_{41}Si_{39}$), the X-ray powder pattern revealed a set of weak satellite reflections that correspond to a tetragonal lattice similar to $ThCr_2Si_2$ with smaller unit cell dimensions. At this point, it was not clear whether the Ni-rich phase $Ce_{20}Ni_{46}Si_{34}$ represents a new phase or the Ni-rich end of a homogeneity range of $ThCr_2Si_2$-type $CeNi_2Si_2$. The amount of the Ni-rich phase $Ce_{20}Ni_{46}Si_{34}$ in the as-cast state increases as the alloy composition shifts towards the Ni-rich side at a constant Ce content, where at an alloy composition of $Ce_{20}Ni_{60}Si_{20}$ a single crystal suitable for X-ray structure analysis (see below) was selected.

3.1.1. The crystal structure of $CeNi_{2+x}Si_{2-x}$, x = 0.33 with the $CaBe_2Ge_2$-type. A single crystal, extracted from an as-cast alloy with a nominal composition of $Ce_{20}Ni_{60}Si_{20}$ revealed unit cell parameters (a = 0.40150(2) and c = 0.95210(2) nm) consistent at first glance with a body centred $ThCr_2Si_2$ type, but additional weak reflections could be satisfactorily indexed on the basis of a primitive Bravais cell. Systematic extinctions suggested the space group type $P4/nmm$ for the highest crystal symmetry. Direct methods indicated Ce, Ni, Si atoms in positions typical for the $CaBe_2Ge_2$-type, where the electropositive atom occupies the 2c site (1/4, 1/4, ~0.75), the transition metal atoms occupy a 2c site (1/4, 1/4, ~0.1) and a 2b site (3/4, 1/4, 1/2), and the tetrel atoms occupy the sites 2c (1/4, 1/4, ~0.35) and 2a (3/4, 1/4, 0). Refinement with anisotropic atom displacement parameters (ADPs) converged to R_F = 0.0163 and residual electron densities smaller than ±1.53 e^- Å^{-3} with fully occupied metal sites but for a statistical occupation of 0.33Ni + 0.67Si in site 2a of $P4/nmm$, which was fixed after the EPMA value. Thus, a structure formula $CeNi_{2+x}Si_{2-x}$, x = 0.33, results, which corresponds to the composition $Ce_{20}Ni_{46.5}Si_{33.5}$ close to the $ThCr_2Si_2$-type phase. Crystal data for $CeNi_{2+x}Si_{2-x}$ along with the ADPs are summarized in Table 1. Although attempts to refine the Ni/Si ratio at the 2a site yield a lower R_F of 0.011 and a residual electron density less than 0.87 e^- Å^{-3}, the resulting Ni content (0.22(1)Ni + 0.78Si) corresponds to the composition $Ce_{20}Ni_{44.5}Si_{35.5}$ deviating significantly from the EPMA derived composition. Thus we prefer the EPMA value and the corresponding formula $CeNi_{2+x}Si_{2-x}$, x = 0.33.

It is worth mentioning that although the primitive reflections in $CaBe_2Ge_2$-type $CeNi_{2+x}Si_{2-x}$ are relatively small, they are still visible in the single-phase powder diffraction spectra. Interestingly, neither a Ni-rich composition nor primitive reflections could be observed at 800 °C in alloys at the Ni-rich side of the 1 : 2 : 2 stoichiometry. This strongly suggests that the primitive $CaBe_2Ge_2$-type phase $CeNi_{2+x}Si_{2-x}$ is a high temperature phase. Alloys at the Ni-rich side of 1 : 2 : 2 annealed at 1000 °C indeed show the Ni-rich composition $Ce_{20}Ni_{\sim 46}Si_{\sim 34}$ in equilibrium with $CeNi_4Si$ and $Ce(Ni_{1-x}Si_x)_3$. Consequently, the X-ray powder diffraction spectra show two sets of $BaAl_4$-type reflections (see Fig. 2). As the sample is multiphase, it is rather difficult to identify the primitive peaks, however, the lattice parameters of one of the $BaAl_4$ derivative phases show a shorter c-axis, which is closer to the value of $CeNi_{2+x}Si_{2-x}$ with the primitive $CaBe_2Ge_2$-type as obtained from the single crystal data. The other set of $BaAl_4$ derivative reflections give similar unit cell parameters as for $CeNi_2Si_2$ with the $ThCr_2Si_2$-type. These observations, together with the fact that a single crystal was obtained from an as-cast alloy led us to conclude that $CeNi_{2+x}Si_{2-x}$ with the primitive $CaBe_2Ge_2$-type is a high temperature phase (1000 °C ≤ $T_{stability}$ < 1615 °C).[36]

Polymorphism between $ThCr_2Si_2$- and $CaBe_2Ge_2$-types is often encountered in various systems, particularly for ternary rare earth silicides containing Ir and Pt.[12] In some cases, *e.g.* in the La–Ir–Si system,[37] the $CaBe_2Ge_2$-type is the high temperature form, whilst the $ThCr_2Si_2$-type is stable at lower temperatures. Therefore $CeNi_{2+x}Si_{2-x}$ with the primitive $CaBe_2Ge_2$-type is hitherto the first example of $ThCr_2Si_2$–$CaBe_2Ge_2$ polymorphism found in ternary rare earth silicides with 3d transition metal elements. The slight flattening of the unit cell, *i.e.* the shorter length of the c-axis observed in $CeNi_{2+x}Si_{2-x}$ ($CaBe_2Ge_2$-type), is also commonly found in many systems exhibiting such polymorphism.[12]

Besides the temperature effect, the substitution of Si by Ni at the 2a-site may act as a driving force for the structural change from a body centred to a primitive atom arrangement in terms of a group–subgroup relation. This idea comes from the fact that an alloy with stoichiometric composition $CeNi_2Si_2$ does not show any changes in the powder diffraction spectra in the as-cast state, and after annealing at 1000 °C for 4 days. An example of structural evolution at a constant temperature can be found in the Sr–Au–Ge system[38] where at 700 °C, increasing the Ge content in $SrAu_{2-x}Ge_{2+x}$ led to a series of structural changes from the $ThCr_2Si_2$-type to the $BaCu_2Sb_2$-type and finally to the $CaBe_2Ge_2$-type, where all structure types are variants of the $BaAl_4$-type.

3.2. The quaternary solution phases $La(Ni_{1-x}Zn_x)_2Si_2$ and $Ce(Ni_{1-x}Zn_x)_2Si_2$

As neither stoichiometric $CeZn_2Si_2$ nor off-stoichiometric $CeZn_{2+x}Si_{2-x}$ ($x \sim 0.5$) exists in the Ce–Zn–Si system at 800 °C,

Table 1 X-ray single crystal data[a] for $CeNi_{2+x}Si_{2-x}$, $x = 0.33$ and X-ray powder diffraction data for $CeNi_2Si_2$ and $LaNi_2Si_2$ (samples annealed at 800 °C)

Compound	$CeNi_{2+x}Si_{2-x}$, $x = 0.33$	$CeNi_2Si_2$	$LaNi_2Si_2$
EMPA composition [at.%]	$Ce_{20.1}Ni_{46.5}Si_{33.4}$	$Ce_{20.4}Ni_{38}Si_{41.6}$	$La_{20.3}Ni_{37.9}Si_{41.8}$
Refinement composition [at.%]	$Ce_{20}Ni_{46.5}Si_{35.5}$	$Ce_{20.0}Ni_{40.0}Si_{40}$	$La_{20.4}Ni_{38.8}Si_{40.8}$
Space group	*P*4/*nmm*; no. 129, origin choice 2	*I*4/*mmm*, no. 139	*I*4/*mmm*, no. 139
Structure type	$CaBe_2Ge_2$	$ThCr_2Si_2$	$ThCr_2Si_2$
Data collection	Nonius Kappa CCD	Guinier image plate	Guinier image plate
Radiation	MoK_α	$CuK_{\alpha1}$	$CuK_{\alpha1}$
θ range	$2.14 < \theta < 36.16$	$10 < 2\theta < 100$	$10 < 2\theta < 100$
Crystal size [μm]	40 × 50 × 50	—	—
a [nm]	0.40150(2)	0.40363(1)	0.41124(1)
c [nm]	0.95210(2)	0.95758(1)	0.97119(1)
Reflections in refinement	$226F_o > 4\sigma(F_o)$ of 262	38	39
Z, volume [nm^3]	2, 0.1535(1)	2, 0.156(1)	2, 0.164(1)
Number of variables	15	22	22
$R_F = \sum\|F_o - F_c\|/\sum F_o$	0.0163	$R_F = 0.024$	$R_F = 0.028$
R_{Int}	0.0107	$R_I = 0.024$	$R_I = 0.028$
GOF	1.195	$\chi^2 = 1.72$	$\chi^2 = 3.09$
Extinction (Zachariasen)	0.044(2)	—	—
RE	Ce in 2c (1/4, 1/4, *z*); $z = 0.75072(4)$;	Ce in 2a (0, 0, 0)	La in 2a (0, 0, 0)
Occ.; $B_{iso.}$	1.00(1); —	1.00(1); 0.14(2)	1.00(1); 0.95(2)
U_{11} [b] = U_{22}; U_{33}; $U_{23} = U_{13} = U_{12} = 0$	0.0057(1); 0.0068(2)	—	—
Ni	Ni1 in 2c (1/4, 1/4, *z*); $z = 0.1264(1)$;	Ni in 4d (0, 1/2, 1/4)	Ni in 4d (0, 1/2, 1/4)
Occ.; $B_{iso.}$	1.00(1); —	1.00(2); 0.60(5)	0.95(2); 0.19(3)
U_{11} [b] = U_{22};U_{33};$U_{23} = U_{13} = U_{12} = 0$	0.0134(3); 0.0120(4)		
Ni; Occ.	Ni2 in 2b (3/4, 1/4, 1/2); 1.00(1)	—	—
U_{11} [b] = U_{22};U_{33};$U_{23} = U_{13} = U_{12} = 0$	0.0085(2); 0.0074(3)	—	—
Si	Si1 in 2c (1/4, 1/4, *z*);	Si in 4e (0, 0, *z*);	Si in 4e (0, 0, *z*);
	$z = 0.3717(2)$;	$z = 0.3804(3)$;	$z = 0.3684(2)$;
Occ.; $B_{iso.}$	1.00(1); —	1.00(1); 0.26(7)	1.00(1); 0.49(5)
U_{11} [b] = U_{22};U_{33}; $U_{23} = U_{13} = U_{12} = 0$	0.0056(4); 0.0077(7)		
M	M in 2a (3/4, 1/4, 0);	—	—
Occ.	0.33(−) Ni3 + 0.67(−) Si2[c]	—	—
U_{11} [b] = U_{22};U_{33};$U_{23} = U_{13} = U_{12} = 0$	0.0163(4); 0.0102(6)	—	—
Residual electron density; max; min in [electrons/nm^3] × 1000	1.18; −1.53	—	—

[a] Crystal structure data are standardized using the program Structure Tidy.[39] [b] Anisotropic atomic displacement parameters U_{ij} in [10^{-2} nm^2]. [c] Fixed after EPMA.

it is interesting to investigate the extent of solubility of Zn in the $CeNi_2Si_2$ phase at 800 °C. Stoichiometric body centred $CeNi_2Si_2$ is found to substitute for Ni up to 18% Zn, *i.e.* $Ce(Ni_{1-x}Zn_x)_2Si_2$, $x = 0.18$. The substitution of Zn for Ni is also reflected in the gradual increase of the unit cell parameters (Fig. 1). For further Zn substitution the Bravais lattice changes from body centered to primitive, as indicated by the appearance of additional weak reflections that violate the systematic extinction of a body-centred cell. The samples remain single phase up to $x = 0.55$ at 800 °C. On further Zn substitution the samples became multiphase, indicating that the solubility limit has been reached.

Since the primitive $CaBe_2Ge_2$-type phase also exists in the Ce–Ni–Si end member system at a high temperature in the Ni-rich side, and the body centred $ThCr_2Si_2$-type phase extends slightly to both the Ni- and Si-rich sides at 800 °C, we suspected that a slight deviation from the stoichiometric 1 : 2 : 2 composition could stabilize/destabilize one of these structure types with the incorporation of Zn. Such a situation is often found in various systems, *e.g.* in the Ce–Zn–Si system at 800 °C [13] or Ce–Ag–Si at 500 °C [40] where two compositional polymorphic modifications of $CeSi_2$ with the α-$ThSi_2$ type and the α-$GdSi_2$ type dissolve transition metal elements, however, the α-$GdSi_2$-based solid solutions end prematurely while the α-$ThSi_2$-based solid solutions extend further up to ~20 at.% transition metal content.

In order to check the possibility of such a scenario we prepared several alloys with off-stoichiometric compositions. Although the nominal compositions deviate far (~5 at.%) from the 1 : 2 : 2 composition, only a small variation (±1 at.%) in the homogeneity range could be observed in the quaternary 122 phase. A variation of unit cell parameters of alloys in both the Si-poor and rich parts of the 122 stoichiometry shows good agreement with those from the stoichiometric 122 alloys. This suggests that there is no parallel solid solution running beside the one shown in Fig. 1.

3.2.1. The crystal structures of $\{La,Ce\}(Ni_{1-x}Zn_x)_2Si_2$ with the $CaBe_2Ge_2$-type. In order to get details on the primitive unit cell, a single crystal has been selected from the flux residuals of an alloy with the composition $Ce_2Ni_4Si_8Zn_{86}$ (in at.%), slowly cooled from 900 °C. A SEM analysis performed directly on the crystals separated from the flux (shown in Fig. 3), defined the composition as $Ce_{19.4}Ni_{25.3}Zn_{16.1}Si_{39.2}$ (at.%). Unit cell, systematic extinctions (indicating *P*4/*nmm* as the space group type of highest symmetry) as well as the X-ray intensity pattern confirmed a structure solution in terms of

the $CaBe_2Ge_2$-type. It should be mentioned, however, that six reflections with $I_{obs} > 4\sigma(I)$ violated the space group extinction rules: (010), (210), (210), (230), (230) and (340). In comparison with the highest intensity observed (12 000 counts), the (210), (210), (230), (230) reflection intensities are below 2 counts and can be disregarded, whereas the (010) intensity (below 7 counts) may stem from a 'Renninger enhancement' effect.

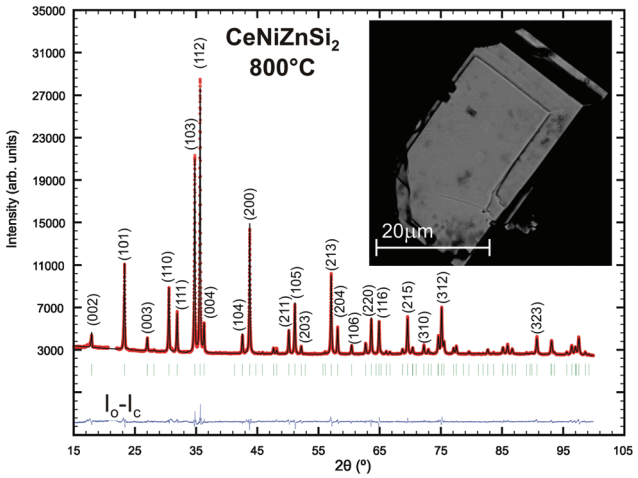

Fig. 3 Rietveld refinement pattern with *hkl* indexes of the alloy with the composition $Ce_{20}Ni_{20}Zn_{20}Si_{40}$ at.% showing $Ce(Ni_{1-x}Zn_x)_2Si_2$ (x = 0.39) with $CaBe_2Ge_2$-type (space group *P4/nmm*) and the micrograph of the single crystal obtained from the Zn flux (sample $Ce_2Ni_4Si_8Zn_{86}$ at.%). Note that the peak at $2\theta \sim 22°$ is from the sample carrier foil.

Interestingly, the site occupation of the transition metal and tetrel atoms is exchanged, *i.e.* the tetrel atoms occupy sites 2c (1/4, 1/4, ~0.1) and 2b, whilst the transition metal atoms occupy sites 2c (1/4, 1/4, ~0.35) and 2a. This site exchange configuration gives rise to the intensity of the primitive reflections, therefore the $CaBe_2Ge_2$-type phases can be identified easily in the quaternary system by X-ray powder diffraction.

Although the small differences in the X-ray scattering power of Ni and Zn make it difficult to unambiguously differentiate between these atom types, it was possible to define the site occupation of Zn by analyzing site ADPs. As the ADPs of the two Si sites did not show any anomalies, it was certain that Zn occupied one or both of the Ni sites. Among all remaining combinations of Zn site occupations, the lowest R_F was found when Zn substituted Ni at the 2a site. Although it was possible to refine the Ni/Zn occupancy at this site, the resulting value (0.48(3)Ni + 0.52Zn) deviates far from the value obtained by EPMA: 0.22Ni + 0.78Zn. Therefore, in the final refinement the Ni/Zn occupancy was fixed according to EPMA, resulting in the structure formula $Ce(Ni_{1-x}Zn_x)_2Si_2$, x = 0.39 (*i.e.* $Ce_{20}Ni_{24.4}Zn_{15.6}Si_{40}$).

The final refinement converged to R_F = 0.0134 and residual electron densities were less than ±1.48 electrons per Å^3 for three metal and two Si positions with a Wyckoff sequence

Table 2 X-ray single crystal data for $Ce(Ni_{1-x}Zn_x)_2Si_2$, x = 0.39 and Rietveld XRPD data for $La(Ni_{1-x}Zn_x)_2Si_2$; x = 0.44 (space group *P4/nmm*; No. 129, origin at center)[a]

Compound	$Ce(Ni_{1-x}Zn_x)_2Si_2$, x = 0.39	$La(Ni_{1-x}Zn_x)_2Si_2$, x = 0.44
EMPA composition [at.%]	$Ce_{19.4}Ni_{25.3}Zn_{16.1}Si_{39.2}$	$La_{19.9}Ni_{22.3}Zn_{17.2}Si_{40.7}$
Refinement composition [at.%]	$Ce_{20}Ni_{24.4}Zn_{15.6}Si_{40}$	$La_{20}Ni_{22.6}Zn_{17.4}Si_{40}$
Structure type	$CaBe_2Ge_2$	$CaBe_2Ge_2$
Data collection	Nonius Kappa CCD	Guinier–Huber IP
Radiation	MoK_α	$CuK_{\alpha1}$
θ range	$2.08 < \theta < 36.05$	$8 < 2\theta < 100$
Crystal size [µm]	40 × 50 × 50	—
a [nm]	0.41022(1)	0.41680(6)[c]
c [nm]	0.98146(4)	0.99213(7)[c]
Reflections in refinement	$266F_o > 4\sigma(F_o)$ of 272	72
Mosaicity	0.65	—
Z, density [gm cm^{-3}]	2, 6.44	2, 6.022
Number of variables	15	26
$R_F = \sum\|F_o - F_c\|/\sum F_o$	0.0134	R_F = 0.043
R_{Int}	0.0135	R_I = 0.025
GOF	1.153	χ^2 = 2.78
Extinction (Zachariasen)	0.024(1)	R_w = 2.75
RE in 2c (1/4, 1/4, z); Occ.	z = 0.73977(3); 1.00(1)	z = 0.73833(7); 1.00(1)
U_{11}[b] = U_{22}; U_{33}; U_{23} = U_{13} = U_{12} = 0	0.0050(1); 0.0058(1)	B_{iso} = 0.28(1)
M in 2a (3/4, 1/4, 0); Occ.	0.78(−)Zn1 + 0.22(−)Ni[d]	0.87(−) Zn1 + 0.13(−) Ni1[d]
U_{11}[b] = U_{22}; U_{33}; U_{23} = U_{13} = U_{12} = 0	0.0099(2); 0.0070(2)	B_{iso} = 0.26(3)
Ni2 in 2c (1/4, 1/4, z); Occ.	z = 0.38514(6); 1.00(1)	z = 0.3883(1); 1.00(1)
U_{11}[b] = U_{22}; U_{33}; U_{23} = U_{13} = U_{12} = 0	0.0063(2); 0.0071(3)	B_{iso} = 0.36(4)
Si1 in 2b (3/4, 1/4, 1/2); Occ.	1.00(1)	1.00(1)
U_{11}[b] = U_{22}; U_{33}; U_{23} = U_{13} = U_{12} = 0	0.0061(3); 0.0060(5)	B_{iso} = 0.54(6)
Si2 in 2c (1/4, 1/4, z); Occ.	z = 0.1474(2); 1.00(1)	z = 0.1537(3); 1.00(1)
U_{11}[b] = U_{22}; U_{33}; U_{23} = U_{13} = U_{12} = 0	0.0106(4); 0.0096(6)	B_{iso} = 0.68(7)
Residual electron density; max; min in [electrons per nm^3] × 1000	1.48; −0.97	

[a] Crystal structure data are standardized using the program Structure Tidy.[39] [b] Anisotropic atomic displacement parameters U_{ij} in [10^{-2} nm^2]. [c] Ge standard. [d] Fixed after EPMA.

abc[3]. Crystal data for $Ce(Ni_{1-x}Zn_x)_2Si_2$, x = 0.39, with the $CaBe_2Ge_2$-type along with the ADPs are summarized in Table 2; interatomic distances are presented in Table 3; coordination polyhedra for all atom sites and a three-dimensional view on the crystal structure are presented in Fig. I of the ESI.‡

The comparison of the structures of $CeNi_{2+x}Si_{2-x}$ and $Ce(Ni,Zn)_2Si_2$ in Fig. 4 clearly reveals an atom site exchange in the tetrahedron-layers sandwiching the Ce-atoms: Ni- and Si-layers are exchanged. However, it is interesting to see that the random substitution of Ni/Si and Ni/Zn always occurs at the same site (2a site).

Several examples of such site exchange variants of the $CaBe_2Ge_2$-structure type can be found in the literature, particularly for ternary stannides and antimonides, *e.g.* Ce{Ni,Cu,Pd,Ir,Pt}$_2$Sn$_2$.[12] For ternary silicides, only the high temperature modification $LaIr_2Si_2$ [37] is known to exhibit such a site exchange arrangement. A similar situation is also encountered in quaternary $Ce(Cu_{1-x}Ag_x)_{2-y}Sb_2$.[41]

In contrast to primitive $Ce(Ni_{1-x}Zn_x)_2Si_2$, where the occupation of Zn/Si sites is inverted with respect to primitive $CeNi_{2+x}Si_{2-x}$, body centred $Ce(Ni_{1-x}Zn_x)_2Si_2$ as well as off-stoichiometric $CeZn_{2+x}Si_{2-x}$ ($x \sim 0.5$) do not exhibit such a site exchange.

The Rietveld refinement performed on single-phase body centred $Ce(Ni_{1-x}Zn_x)_2Si_2$ (x = 0.18) shows that Zn substitutes Ni at the 4d site, while the 4e site remains fully occupied by Si. In the case of ternary $CeZn_{2+x}Si_{2-x}$ (x = 0.5), due to the higher Zn-content, Zn and Si share the 4e site with a ratio of 3 : 7 whereas the 4d site is fully occupied by Zn.[14] A detailed group–subgroup diagram relating the parent $BaAl_4$ structure to the $ThCr_2Si_2$ and $CaBe_2Ge_2$ for the various phases in the Ce–Ni–Zn–Si system is presented in terms of a Bärnighausen tree, depicted in Fig. II of the ESI.‡

In analogy to the section $Ce(Ni_{1-x}Zn_x)_2Si_2$, phase relations have also been explored for the isopleth $La(Ni_{1-x}Zn_x)_2Si_2$ (see Fig. 1). Combined EPM and X-ray powder intensity data analyses revealed a solid solution with the $ThCr_2Si_2$-type for $0 \leq x \leq 0.125$, followed by a change to a primitive tetragonal symmetry typical for the $CaBe_2Ge_2$-type for $0.25 \leq x \leq 0.55$. The solid solution terminates at x = 0.55 as for higher Zn-concentrations multiphase X-ray spectra were observed. Rietveld refinement data for $La(Ni_{0.56}Zn_{0.44})_2Si_2$ are summarized in Table 2 and Fig. 5.

Table 3 Interatomic distances for $Ce(Ni_{1-x}Zn_x)_2Si_2$, x = 0.39 (*P4/nmm*; no. 129). Standard deviations <0.00007

Atom 1	Atom 2	$d_{1,2}$ [nm]
Ce1	Si2 (4×)	0.31047
	Si1 (4×)	0.31217
	Ni2 (4×)	0.31491
	M (4×)	0.32757
M	Si2 (4×)	0.25102
	M (4×)	0.29007
	Ce1 (4×)	0.32757
Ni2	Si2 (1×)	0.23329
	Si1 (4×)	0.23405
	Ce1 (4×)	0.31491
Si1	Ni2 (4×)	0.23405
	Si1 (4×)	0.29007
	Ce1 (4×)	0.31217
Si2	Ni2 (1×)	0.23329
	M (4×)	0.25102
	Ce1 (4×)	0.31047

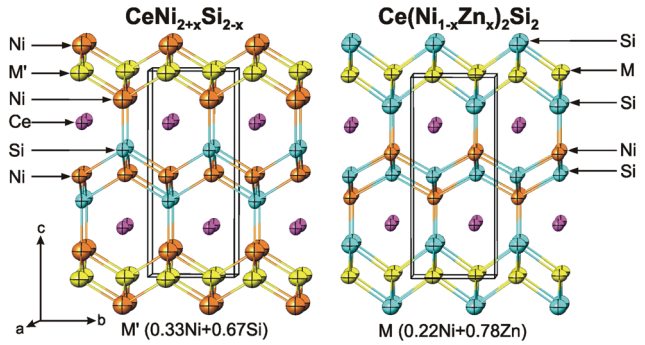

Fig. 4 Atom site distribution for ternary $CeNi_{2+x}Si_{2-x}$ ($CaBe_2Ge_2$-type; left) and atom site exchange arrangement in isopointal quaternary $Ce(Ni_{1-x}Zn_x)_2Si_2$ ($CaBe_2Ge_2$-type; right). Atoms are presented with ADPs from single crystal refinement.

3.3. Physical properties of $La(Ni_{1-x}Zn_x)_2Si_2$ and $Ce(Ni_{1-x}Zn_x)_2Si_2$

Two samples, {La,Ce}(Ni,Zn)$_2$Si$_2$ were selected from the solid solution to check on the physical properties of this series.

3.3.1. $La(Ni_{1-x}Zn_x)_2Si_2$. $La(Ni_{1-x}Zn_x)_2Si_2$, x = 0.44 was studied down to 400 mK, but no phase transition, indicating *e.g.*, superconductivity was observed. The temperature dependent heat capacity, C_p, of $La(Ni_{0.56}Zn_{0.44})_2Si_2$ is shown in Fig. 6(a) and plotted as C_p/T *vs.* T. Unexpectedly, $C_p/T(T)$ exhibits a minimum around 2.5 K below which the electronic con-

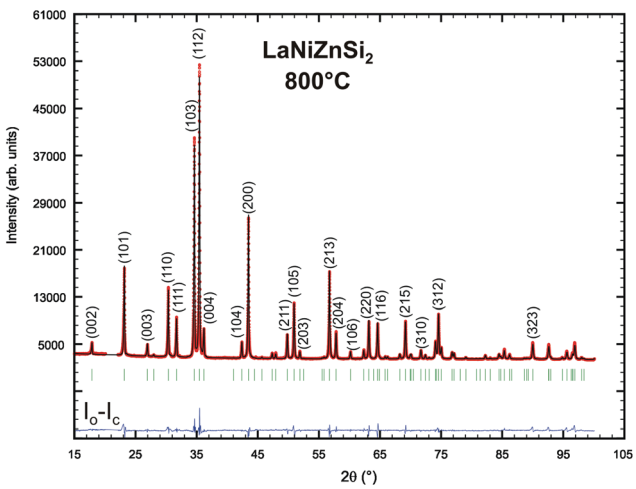

Fig. 5 Rietveld refinement pattern with *hkl* indexes of single phase $La(Ni_{1-x}Zn_x)_2Si_2$; x = 0.44 ($CaBe_2Ge_2$-type, space group *P4/nmm*) from the alloy with nominal composition $La_{20}Ni_{20}Zn_{20}Si_{40}$ at.%, annealed at 800 °C.

tribution tends towards 20 mJ mol^{-1} K^{-2} for $T \sim 0$, a value larger than what is likely for simple intermetallic compounds. The overall shape, however, reminds one of spin fluctuation systems like YCo_2 or UAl_2.[42] In order to prove such a proposition, the standard spin fluctuation ansatz, $C_p(T) = \gamma T + \beta T^3 + \delta T^3 \ln(T/T^*)$ is employed to the experimental data, revealing excellent agreement for γ = 13 mJ mol^{-1} K^{-2} and T^* = 8.7 K (solid line, inset Fig. 6(a)). This agreement would suggest spin fluctuations in the nearly localized regime present in $La(Ni_{0.56}Zn_{0.44})_2Si_2$. The fit parameter β = 0.13 mJ mol^{-1} K^{-4} allows the estimation of a Debye temperature of about 460 K, referring to the rather stiff lattice of this system.

The resistivity, ρ, of $La(Ni_{0.56}Zn_{0.44})_2Si_2$ was studied within the temperature range 4.2–300 K. At elevated temperatures ($T >$ 100 K) $\rho(T)$ behaves metallic-like. The almost linear slope of $\rho(T)$ refers predominantly to electron–phonon interactions. A shallow minimum is observed at about 25 K and below this temperature the resistivity increases with decreasing temperature (see Fig. 6(b)). A plot of the resistivity on a logarithmic temperature scale (inset, Fig. 6(b)) for various externally applied magnetic fields reveals, unexpectedly a logarithmic behaviour, indicating Kondo-type interactions, which might be attributed to a small amount of uncompensated Ni spins. These features were reproduced in several independently prepared samples and comply with the enhanced value of the Sommerfeld constant deduced from the specific heat experiment.

3.3.2. $Ce(Ni_{1-x}Zn_x)_2Si_2$. Fig. 7–9 reveal experimental results regarding the magnetic properties of $Ce(Ni_{1-x}Zn_x)_2Si_2$, x = 0.39. Ce in its atomistic form possesses one electron in the 4f shell, constituting the 4f^1 electronic configuration (EC) and thus carries a total angular momentum j = 5/2. This gives rise to a non-vanishing magnetic moment. In the case of cerium and ytterbium compounds, however, partial hybridisation with the conduction electron system is possible. Its degree depends on the compound's specific electronic structure and in solid solutions on the local chemical environment, *i.e.*, Ce moments varying with the Ni/Zn random occupation in the title compound.

A simple proof of whether or not this EC is preserved in the solid state of $Ce(Ni_{0.61}Zn_{0.39})_2Si_2$ can be obtained from temperature dependent magnetic measurements. The inverse magnetic susceptibility at 3 T is shown in Fig. 7(a). Phase transitions above 2.5 K are not obtained from this measurement. A quantitative description of the high temperature magnetic susceptibility (50–300 K) can be made by applying a modified Curie Weiss law, revealing a temperature independent Pauli susceptibility (χ_0 = 3.9 × 10^{-4} emu mol^{-1}), an effective magnetic moment, which is related to the Curie constant (μ_{eff} = 2.20μ_B/Ce) and a paramagnetic Curie temperature (θ_p = −35 K) from a least squares fit of this model to the experimental data (solid line, Fig. 7(a)).

A negative paramagnetic Curie temperature, in general, refers to antiferromagnetic interactions between conduction electrons and the almost localized Ce 4f electrons. Crystalline electric field (CEF) effects, lifting the $2j + 1 = 6$ fold degenerate ground state, as well as the Kondo effect, modify, however, the absolute value of θ_p. The effective magnetic moment observed from the Curie Weiss law is below that (2.54μ_B) expected for the free ion Ce^{3+} state (EC: 4f^1). This reduction may be caused by the fraction of Ce ions in the Ni richer environments, whereas Zn tends to stabilise the Ce^{3+} local moment character.

The slight curvature observed in the $1/\chi$ *vs.* T data-set might result from CEF effects which are simply modelled here by adjusting the parameter χ_0. At temperatures below about 2 K, the susceptibility, $\chi(T)$, displays a smooth cross-over from the high temperature Curie–Weiss behaviour towards a low temperature Kondo-like flattening of the susceptibility which reaches a value χ_{LT} = 0.054 emu mol^{-1} at 0.7 K (see inset in Fig. 9b).

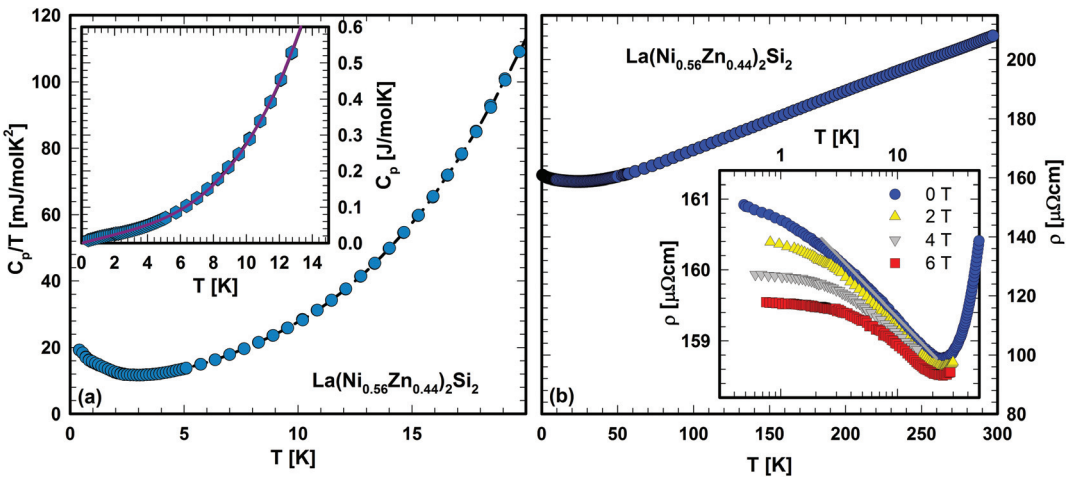

Fig. 6 (a) Temperature dependent specific heat C_p of $La(Ni_{0.56}Zn_{0.44})_2Si_2$ plotted as C_p/T *vs.* T. The inset shows the data as C_p *vs.* T. The solid line is a least squares fit according to the spin fluctuation model (see text). (b) Temperature dependent electrical resistivity ρ of $La(Ni_{0.56}Zn_{0.44})_2Si_2$. The inset shows the low temperature resistivity data on the logarithmic temperature scale for various magnetic fields. The logarithmic temperature dependence is highlighted by the solid line.

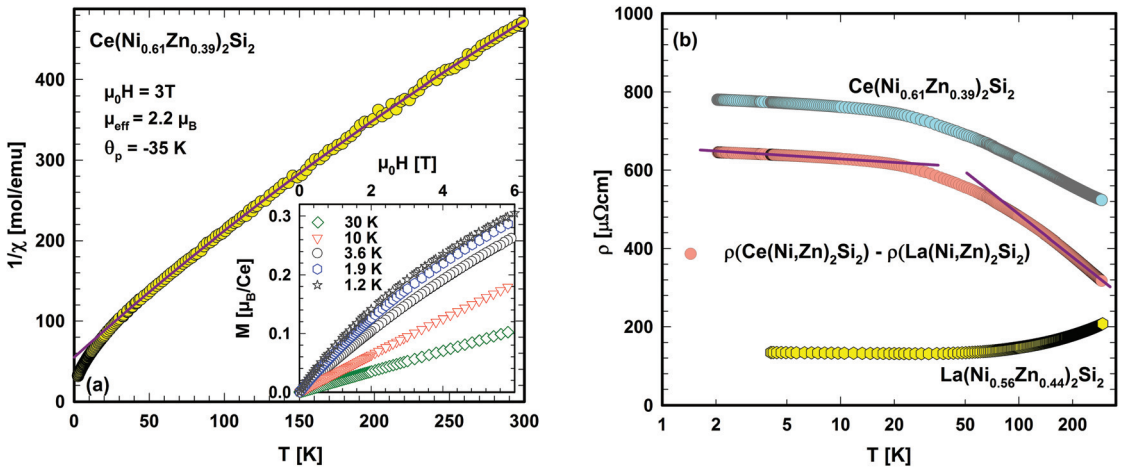

Fig. 7 (a) Temperature dependent magnetic susceptibility χ of $Ce(Ni_{0.61}Zn_{0.39})_2Si_2$ plotted as $1/\chi$ *vs.* T. The solid line is the result of a least squares fit of the modified Curie Weiss law to the experimental data above 50 K. The inset shows the field dependent magnetization of $Ce(Ni_{0.61}Zn_{0.39})_2Si_2$ for various temperatures. (b) Temperature dependent electrical resistivity ρ of $Ce(Ni_{0.61}Zn_{0.39})_2Si_2$ and $La(Ni_{0.56}Zn_{0.44})_2Si_2$. The magnetic contribution to the electrical resistivity, ρ_{mag}, of $Ce(Ni_{0.61}Zn_{0.39})_2Si_2$ is shown as well. The solid lines are guides for the eyes.

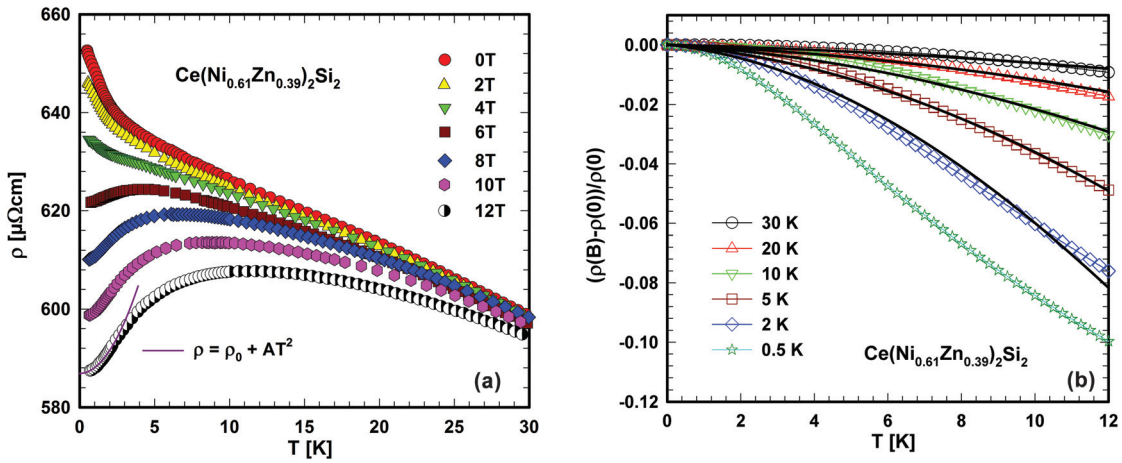

Fig. 8 (a) Low temperature electrical resistivity ρ of $Ce(Ni_{0.61}Zn_{0.39})_2Si_2$ for various externally applied magnetic fields. The solid line is a least squares fit as explained in the text. (b) Field dependent magnetoresistance $(\rho(B) - \rho(0))/\rho(0)$ of $Ce(Ni_{0.61}Zn_{0.39})_2Si_2$ for various temperatures. $\rho(B)$ and $\rho(0)$ are the field and the zero field resistivities. The solid lines correspond to numerical calculations according to Schlottmann's theory.[45]

The inset in Fig. 7(a) shows isothermal magnetization curves, M, for $Ce(Ni_{0.61}Zn_{0.39})_2Si_2$ measured at temperatures ranging from 1.2 K to 30 K. Neither spontaneous magnetization nor metamagnetic-like features are obvious from these measurements, thus excluding long range magnetic order in the measured temperature range. A smooth, slightly curvilinear $M(H)$ dependence at low temperatures is observed with relatively small magnetization values near $0.3\mu_B$/Ce at 1.2 K and 6 T. A combination of both, CEF splitting and the Kondo effect (see below) is expected to be responsible for the magnitude of the low temperature magnetic moment.

Fig. 7(b) shows the temperature dependent electrical resistivity, ρ, of $Ce(Ni_{0.61}Zn_{0.39})_2Si_2$ in comparison with that of $La(Ni_{0.56}Zn_{0.44})_2Si_2$. In distinct contrast to $\rho(T)$ of $La(Ni_{0.56}Zn_{0.44})_2Si_2$, the electrical resistivity of $Ce(Ni_{0.61}Zn_{0.39})_2Si_2$ evidences a negative value of $d\rho/dT$ in the entire temperature range. Additionally, much larger $\rho(T)$ values are observed as a consequence of additional magnetic scattering processes. If $\rho(T)$ of $La(Ni_{0.56}Zn_{0.44})_2Si_2$ is assumed to primarily derive from electron–phonon interactions, besides a constant residual resistivity, the magnetic scattering processes of electrons on the 4f moments of Ce can be isolated by simply subtracting the resistivity curve of $La(Ni_{0.56}Zn_{0.44})_2Si_2$ from that of $Ce(Ni_{0.61}Zn_{0.39})_2Si_2$. Results are shown in Fig. 7(b) on a semi-logarithmic temperature scale. Obviously, two temperature ranges can be identified, where $\rho_{mag}(T)$ behaves in a negative-logarithmic manner (see the solid lines in Fig. 7(b) as a guide for the eyes). Such a behaviour is a hallmark of Kondo-type interactions, as present in a huge amount of cerium based compounds. Following the preposition of

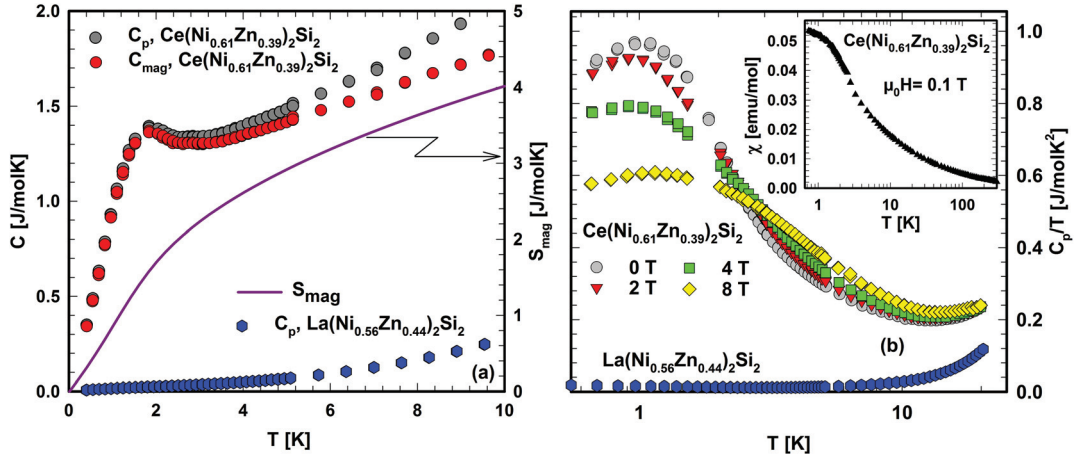

Fig. 9 (a) Temperature dependent specific heat C_p of $Ce(Ni_{0.61}Zn_{0.39})_2Si_2$ and $La(Ni_{0.56}Zn_{0.44})_2Si_2$. $C_{mag}(T)$ is derived by subtracting both data-sets. The temperature dependent magnetic entropy S_{mag} (solid line, referring to the right axis) originates from the integration of $C_{mag}/T(T)$. (b) Field and temperature dependent heat capacity data of $Ce(Ni_{0.61}Zn_{0.39})_2Si_2$ plotted as C_p/T *vs.* log T for various externally applied magnetic fields. Data of $La(Ni_{0.56}Zn_{0.44})_2Si_2$ are added for the purpose of comparison. The inset shows the low temperature magnetic susceptibility data measured at 0.1 T and temperatures down to 0.7 K.

Cornut and Coqblin[43] the logarithmic resistivity ranges at low and high temperatures can be understood as derived from the Kondo effect in the CEF ground state and in an excited CEF state, respectively. If these levels are well separated in energy, a pronounced maximum in $\rho_{mag}(T)$ would be expected as well. Overall, the present resistivity study strongly indicates a Kondo effect existing in $Ce(Ni_{0.61}Zn_{0.39})_2Si_2$.

In general, a lattice of Kondo ions (*i.e.*, a Kondo lattice) is characterised by a drop of the electrical resistivity at lowest temperatures due to coherence. A distribution of Kondo temperatures due to random Ni/Zn occupation may inhibit the formation of a coherent state at low temperatures in the present system (compare Fig. 7b and 8a). Externally applied magnetic fields tend to suppress incoherent scattering processes. Accordingly, for fields above about 6 T, a smooth maximum forms in $\rho(T)$, which shifts continuously to higher temperatures. Such behaviour can be understood in terms of a Kondo lattice, where the maximum in $\rho(T)$ is a measure of the Kondo temperature.[44] At lowest temperatures, a Kondo lattice exhibits a Fermi liquid ground state documented by the T^2 behaviour of the electrical resistivity (solid line, Fig. 8(a)). Isothermal resistivity data at various external fields, as presented in Fig. 8(b), reveal a moderate negative magnetoresistance, amounting to about 10% at lowest temperatures and 12 T.

The overall negative magnetoresistance is in line with the Kondo behaviour, where increasing magnetic fields suppress Kondo interactions and as a result decrease resistivity. Although the field dependence of $(\rho(B) - \rho(0))/\rho(0)$ complies with numerical results employing Schlottmann's theory[45] (solid lines, Fig. 8(b)), the Kondo temperature inferred from such fits appears to be unphysically high (about 50 K) which may be a consequence of the aforementioned site-dependent hybridisation/Kondo interaction strength.

In Fig. 9 the heat capacity data of $Ce(Ni_{0.61}Zn_{0.39})_2Si_2$, measured down to 400 mK, are displayed as C_p *vs.* T. For comparison, $C_p(T)$ of $La(Ni_{0.56}Zn_{0.44})_2Si_2$ is added, too. Below 2 K, the specific heat of $Ce(Ni_{0.61}Zn_{0.39})_2Si_2$ shows an anomaly, which is attributed to Kondo-type interactions and is in close correspondence with the smooth cross-over behaviour displayed by the low temperature magnetic susceptibility shown in the inset of Fig. 9b. In order to calculate the magnetic entropy, released at low temperatures, the specific heat data of $La(Ni_{0.56}Zn_{0.44})_2Si_2$ are assumed to represent the phonon contribution to this quantity, *i.e.*, $C_{mag} = C(Ce(Ni_{0.61}Zn_{0.39})_2Si_2) - C(La(Ni_{0.56}Zn_{0.44})_2Si_2)$. Results of this procedure are shown in Fig. 9(a) as well. Integrating C_{mag}/T from zero to the upper limit of the present measurements reveals the temperature dependent magnetic entropy, S, shown as a solid line in Fig. 9(a). At 3.9 K, the entropy reaches $0.45R\ln 2$ which according to Desgranges and Schotte,[46] corresponds to a Kondo temperature T_K = 3.9 K. As is obvious from Fig. 9(a), $S(T)$ continuously increases, finally reaching a value of $R\ln 2$ around 20 K. The response of the system to the application of magnetic fields is shown in Fig. 9(b), where the heat capacity data are plotted as C_p/T *vs.* log T. The overall observation that C_p/T becomes reduced by magnetic fields, concomitant with an entropy transfer to higher temperatures, is in line with a typical Kondo scenario.

Comparing the absolute numbers of the low temperature Sommerfeld coefficient ($\gamma = C_p/T$) and of the susceptibility χ_{LT}, the value of the Wilson ratio, $R = \pi^2 k_B{}^2\chi_{LT}/[g_J{}^2 J(J+1)\mu_B{}^2\gamma] \sim 2$, provides a further proof that a Kondo screened ground-state CEF doublet dominates the low temperature physics of $Ce(Ni_{0.61}Zn_{0.39})_2Si_2$.

Finally, it is interesting to see that the substitution of Ni by Zn in $CeNi_2Si_2$ at 800 °C supports the $ThCr_2Si_2$-type only up to $Ce(Ni_{0.82}Zn_{0.18})_2Si_2$, where a transition to an atom site occupation variant with the $CaBe_2Ge_2$-type is observed extending up to a composition $Ce(Ni_{0.45}Zn_{0.55})_2Si_2$ and maintaining the stoichiometry $Ce(Ni,Zn)_2Si_2$. At higher Zn contents the

$ThCr_2Si_2$-type reappears at temperatures below 800 °C in the form of $CeZn_2(Si_{0.7}Zn_{0.3})_2$ where Zn-atoms are found to enter the Si-site. It should be noted that Zn atoms in the Ni/Zn substitution enlarge the volume and concomitantly introduce a higher electron/atom ratio. Both facts provide the basis for a gradual change from the intermediate valent Ce in $CeNi_2Si_2$ with a characteristic Kondo-lattice temperature $T^* \sim 600$ K (ref. 21–26) towards a localised magnetic behaviour of Ce in $CeZn_2$-$(Si_{0.7}Zn_{0.3})_2$ with a ground state close to trivalent Ce ($\mu_{eff} = 2.34\mu_B$).[14] Intermediate compositions such as $Ce(Ni_{0.61}Zn_{0.39})_2Si_2$ exhibit a Kondo-type ground state.

4. Conclusions

Although the systems La–Zn–Si and Ce–Zn–Si at 800 °C do not contain a compound "{La,Ce}Zn_2Si_2", solid solutions exist starting from $CeNi_2Si_2$ by the addition of Zn which substitutes Ni. This homogeneity range has been studied for {La,Ce}-$(Ni_{1-x}Zn_x)_2Si_2$, $0 \le x \le 0.55$. Single crystal X-ray diffraction data define the CaB_2Ge_2-type for the crystals of the compounds $Ce(Ni_{0.61}Zn_{0.39})_2Si_2$ (*P*4/*nmm*; $a = 0.41022(1)$ nm, $c = 0.98146(4)$ nm) and $CeNi_{2+x}Si_{2-x}$, $x = 0.33$ (*P*4/*nmm*; $a = 0.40150(2)$ nm, $c = 0.95210(2)$ nm). Whilst the quaternary CaB_2Ge_2-type phase is stable at 800 °C, a reinvestigation of the Ce–Ni–Si system near the stoichiometric composition 1 : 2 : 2 revealed that the CaB_2Ge_2-type phase exists only at high temperatures (≥1000 °C) in the Ni-rich side. Bravais lattice changes from body centered to primitive have been observed at 800 °C starting from $Ce(Ni_{1-x}Zn_x)_2Si_2$ ($0 \le x \le 0.18$) *I*4/*mmm* to $Ce(Ni_{1-x}Zn_x)_2Si_2$, $0.25 < x \le 0.55$, *P*4/*nmm*, however, on further Zn substitution the stability of the 1 : 2 : 2 phase is reduced (<695 °C) and it exists only with an excess amount of Zn as $CeZn_2(Si_{1-x}Zn_x)_2$ with the $ThCr_2Si_2$ type.

The effective paramagnetic moment of Ce in $Ce(Ni_{0.61}Zn_{0.39})_2Si_2$ suggests that the ground state of the Ce ions in this compound is close to trivalent. Enhanced values of the electronic contribution to the specific heat, a Curie–Weiss to Kondo-type cross-over behaviour of the low temperature susceptibility and pronounced ranges of negative logarithmic temperature dependences of the electrical resistivity reveal the presence of the Kondo effect in this cerium compound, in the context of a Wilson ratio, $R \sim 2$. Unexpectedly, $La(Ni_{0.56}Zn_{0.44})_2Si_2$ exhibits a spin fluctuation scenario at low temperatures together with a distinct minimum of the temperature dependent electrical resistivity which we, presumably, interpret as a Kondo effect due to a very low concentration of uncompensated nickel spins.

Acknowledgements

Z. Malik acknowledges the support from the Higher Education Commission of Pakistan (HEC) under the scholarship scheme "PhD in Natural & Basic Sciences from Austria". F. Failamani is thankful for the support from the Austrian Federal Ministry of Science and Research (BMWF) under the scholarship scheme: Technology Grant Southeast Asia (PhD) in the frame of the ASEA UNINET. We thank Dr S. Puchegger for his expert assistance in EPMA measurements and Dr N. Ponweiser and P. Wibner for their contributions to Ce–Ni–Si at the early stage of this work. Support by the FWF P24380 is acknowledged.

References

1 K. R. Andress and E. Alberti, *Z. Metallkd.*, 1935, 27.
2 Z. Ban and M. Sikirica, *Acta Crystallogr.*, 1965, **18**, 594–599.
3 O. S. Zarechnyuk, P. I. Kripyakevich and E. I. Gladyshevskii, *Kristallografiya*, 1965, **9**, 706–708.
4 B. Eisenmann, N. May, W. Müller and H. Schäfer, *Z. Naturforsch., B*, 1972, **27**, 1155–1157.
5 W. Dörrscheidt and H. Schäfer, *J. Less-Common Met.*, 1978, **58**, 209–216.
6 E. Parthé, B. Chabot, H. F. Braun and N. Engel, *Acta Crystallogr., Sect. B: Struct. Sci.*, 1983, **39**, 588–595.
7 O. I. Bodak and E. I. Gladyshevskii, *Izv. Akad. Nauk SSSR, Neorg. Mater.*, 1969, **5**, 2060–2065.
8 O. I. Bodak, M. G. Mis'kiv, A. T. Tyvanchuk, O. I. Kharchenko and E. I. Gladyshevskii, *Izv. Akad. Nauk SSSR, Neorg. Mater.*, 1973, **9**, 864–866.
9 B. Chabot and E. Parthé, *J. Less-Common Met.*, 1984, **97**, 285–290.
10 E. R. Hovestreydt, *J. Less-Common Met.*, 1984, **102**, L27–L29.
11 F. Merlo, M. L. Fornasini and M. Pani, *J. Alloys Compd.*, 2005, **387**, 165–171.
12 P. Villars and K. Cenzual, *Pearson's Crystal Data–Crystal Structure Database for Inorganic Compounds, release 2014/15*, ASM International, Materials Park, OH, USA, 2014.
13 Z. Malik, A. Grytsiv, P. Rogl and G. Giester, *Intermetallics*, 2013, **36**, 118–126.
14 F. Failamani, A. Grytsiv, R. Podloucky, H. Michor, E. Bauer, P. Brož, G. Giester and P. Rogl, *RSC Adv.*, 2015, **5**, 36480–36497.
15 F. Steglich, J. Aarts, C. D. Bredl, W. Lieke, D. Meschede, W. Franz and H. Schäfer, *Phys. Rev. Lett.*, 1979, **43**, 1892–1896.
16 M. Rotter, M. Tegel, D. Johrendt, I. Schellenberg, W. Hermes and R. Pöttgen, *Phys. Rev. B: Condens. Matter*, 2008, **78**, 020503.
17 M. Rotter, M. Tegel and D. Johrendt, *Phys. Rev. Lett.*, 2008, **101**, 107006.
18 A. S. Sefat, R. Jin, M. A. McGuire, B. C. Sales, D. J. Singh and D. Mandrus, *Phys. Rev. Lett.*, 2008, **101**, 117004.
19 E. Bauer, R. T. Khan, H. Michor, E. Royanian, A. Grytsiv, N. Melnychenko-Koblyuk, P. Rogl, D. Reith, R. Podloucky, E.-W. Scheidt, W. Wolf and M. Marsman, *Phys. Rev. B: Condens. Matter*, 2009, **80**, 064504.
20 F. Kneidinger, E. Bauer, I. Zeiringer, P. Rogl, C. Blaas-Schenner, D. Reith and R. Podloucky, *Phys. C*, 2015, **514**, 388–398.

21 G. Knebel, M. Brando, J. Hemberger, M. Nicklas, W. Trinkl and A. Loidl, *Z. Phys. B: Condens. Matter*, 1999, **259–261**, 399–400.
22 E. V. Sampathkumaran and R. Vijayaraghavan, *Phys. Rev. Lett.*, 1986, **56**, 2861–2864.
23 M. Koterlyn, I. Shcherba, R. Yasnitskii and G. Koterlyn, *J. Alloys Compd.*, 2007, **442**, 176–179.
24 T. Toliński, K. Synoradzki, M. Koterlyn, G. Koterlyn and R. Yasnitskii, *J. Alloys Compd.*, 2013, **580**, 512–516.
25 R. K. Singhal, N. L. Saini, K. B. Garg, J. Kanski, L. Ilver, P. O. Nilsson, R. Kumar and L. C. Gupta, *J. Phys.: Condens. Matter*, 1993, **5**, 4013.
26 M. Bertin Tchoula Tchokonté, P. de Villiers du Plessis, A. M. Strydom, T. B. Doyle, S. Ghosh and D. Kaczorowski, *J. Phys. Chem. Solids*, 2015, **77**, 56–61.
27 E. M. Levin, O. I. Bodak, E. I. Gladyshevskii and V. G. Sinyushko, *Phys. Status Solidi A*, 1992, **134**, 107–117.
28 J. Rodriguez-Carvajal, *FULLPROF, a program for Rietveld refinement and pattern matching analysis, Abstract of the satellite meeting on powder diffraction of the XV congress*, Int. Union of Crystallography, Talence, France, 1990, p. 127; see also; J. Rodriguez-Carvajal, *Physica B*, 1993, **55**, 192–194.
29 *Nonius Kappa CCD Program Package COLLECT, DENZO, SCALEPACK, SORTAV*, Nonius Delft, The Netherlands, 1998.
30 G. M. Sheldrick, *Acta Crystallogr., Sect. A: Fundam. Crystallogr.*, 2007, **64**, 112–122.
31 L. J. Farrugia, *J. Appl. Crystallogr.*, 1999, **32**, 837–838.
32 M. Falmbigl, F. Kneidinger, A. Grytsiv, H. Michor, H. Müller, P. Rogl, E. Bauer, G. Hilscher and G. Giester, *Intermetallics*, 2013, **42**, 45–51; see also: F. Kneidinger, H. Michor, A. Sidorenko, E. Bauer, I. Zeiringer, P. Rogl, C. Blaas-Schenner, D. Reith and R. Podloucky, *Phys. Rev. B: Condens. Matter*, 2013, **88**, 104508.
33 H. Zhou, Q. Yao, S. Yuan, J. Liu and H. Deng, *J. Alloys Compd.*, 2004, **366**, 161–164.
34 O. I. Bodak, E. I. Gladyshevskii and P. I. Kripyakevich, *Izv. Akad. Nauk SSSR, Neorg. Mater.*, 1966, **2**, 2151–2155.
35 A. V. Morozkin, A. V. Knotko, V. O. Yapaskurt, F. Yuan, Y. Mozharivskyj and R. Nirmala, *J. Solid State Chem.*, 2013, **208**, 9–13.
36 A. V. Morozkin, Y. D. Seropegin, A. V. Gribanov, I. A. Sviridov, J. M. Kurenbaeva and A. L. Kurenbaev, *J. Alloys Compd.*, 1998, **264**, 190–196.
37 H. F. Braun, N. Engel and E. Parthé, *Phys. Rev. B: Condens. Matter*, 1983, **28**, 1389–1395.
38 I. Zeiringer, A. Grytsiv, E. Bauer, G. Giester and P. Rogl, *Z. Anorg. Allg. Chem.*, 2015, **641**, 1404–1421.
39 L. M. Gelato and E. Parthé, *J. Appl. Crystallogr.*, 1987, **20**, 139–143.
40 B. Belan, O. Bodak, R. Gladyshevskii, I. Soroka, B. Kuzhel, O. Protsyk and I. Stets, *J. Alloys Compd.*, 2005, **396**, 212–216.
41 A. Guzik and E. Talik, *J. Alloys Compd.*, 2002, **346**, 10–16.
42 K. Ikeda, S. K. Dhar, M. Yoshizawa and K. A. Gschneidner Jr., *J. Magn. Magn. Mater.*, 1991, **100**, 292–321.
43 B. Cornut and B. Coqblin, *Phys. Rev. B: Solid State*, 1972, **5**, 4541–4561.
44 D. L. Cox and N. Grewe, *Z. Phys. B: Condens. Matter*, 1988, **71**, 321–340.
45 P. Schlottmann, *Phys. Rev. B: Condens. Matter*, 1982, **25**, 4815–4827, see also: P. Schlottmann, *Phys. Rev. B: Condens. Matter*, 1982, **25**, 4828, and P. Schlottmann, *Phys. Rev. B: Condens. Matter*, 1982, **25**, 4838.
46 H.-U. Desgranges and K. D. Schotte, *Phys. Lett. A*, 1982, **91**, 240–242.